Monthly Notices
of the
ROYAL ASTRONOMICAL SOCIETY

MNRAS **479,** 961–972 (2018) doi:10.1093/mnras/sty1561

Identification and analysis of the young population in the starburst galaxy NGC 253

M. J. Rodríguez,[1]★ G. Baume[1,2] and C. Feinstein[1,2]

[1] *Instituto de Astrofísica de La Plata (CONICET-UNLP), Paseo del bosque S/N, La Plata (B1900FWA), Argentina*
[2] *Facultad de Ciencias Astronómicas y Geofísicas - Universidad Nacional de La Plata, Paseo del bosque S/N, La Plata (B1900FWA), Argentina*

Accepted 2018 June 7. Received 2018 May 14; in original form 2017 May 30

ABSTRACT

We present a study of the young population in the starburst galaxy NGC 253. In particular, we focused our attention on searching for young star groups, obtaining their main properties and studying their hierarchical organization. For this task, we used multiband images and their corresponding photometric data obtained with the Advanced Camera for Surveys of the *Hubble Space Telescope* (ACS/*HST*). We first derived the absorption affecting the different regions of the galaxy. Then, we applied an automatic and objective searching method over the corrected data in order to detect young star groups. We complemented this result with the construction of a stellar density map for the blue young population. A statistical procedure to decontaminate the photometric diagrams from field stars was applied over the detected groups and we estimated their fundamental parameters. As a result, we built a catalogue of 875 newly identified young groups with their main characteristics, including coordinates, sizes, estimated number of members, stellar densities, luminosity function (LF) slopes and galactocentric distances. We observed that these groups delineate different structures of the galaxy, and they are the last step in the hierarchical way in which the young population is organized. From their size distribution, we found they have typical radii of ∼40−50pc. These values are consistent with those found in other nearby galaxies. We estimated a mean value for the LF slope of 0.21 and an average density of 0.0006 star pc^{-3} for the identified young groups, taking into account stars earlier than B6.

Key words: stars: early-type – stars: luminosity function, mass function – galaxies: individual: NGC 253 – galaxies: star clusters: general – galaxies: structure – galaxies: star formation.

1 INTRODUCTION

Young star groups exist in a wide range of sizes, from compact star clusters to star complexes going through OB associations. Young open clusters contain a few tens to 10^5 stars in a typical diameter of a few parsecs and they are gravitationally bound (Moraux 2016). OB associations are composed of young massive stars formed from the same molecular cloud; they are gravitationally unbound with low densities.

The distribution and properties of these systems are useful to understand the most recent history of the host galaxy as well as the star-formation process in different environments. For this reason, in recent decades several works have focused on performing global studies and assembling catalogues of young stars groups over the nearest galaxies: LMC (Gouliermis et al. 2003), SMC (Battinelli 1991), M 31 (Bianchi et al. 2012), M 33 (Chandar, Bianchi & Ford 1999; Bedin et al. 2005), NGC 6347 (Massi et al. 2015), NGC 300 (Pietrzyński et al. 2001; Rodríguez, Baume & Feinstein 2016), NGC 7793 (Pietrzyński et al. 2005), M 81 (Nantais et al. 2010), and M 101 (Bresolin, Kennicutt & Stetson 1996), to name just a few.

In particular, the Sculptor Group galaxy, NGC 253, is a barred almost-edge-on spiral galaxy (SAB(s)c D, Vučetić, Arbutina & Urošević 2015), at a distance of 3.56 Mpc (Tully et al. 2013), which corresponds to a projected linear scale of ∼ 17 pc arcsec^{-1}. One of its most outstanding features is the starburst activity. Different works indicate that these bursts are located in the galactic central region up to ∼ 300 pc in radius, with a star-formation rate (SFR) of ∼ 2–3 $M_\odot$ yr^{-1} (Radovich, Kahanpää & Lemke 2001; Ott et al. 2005); however, their nature is not yet well understood. According to Engelbracht et al. (1998), the bursts are caused by the presence of the bar, which drives the gas into the central region. Additionally, Davidge (2010) suggested that an interaction with a now-defunct companion occurred within the past ∼0.2 Gyr, stimulating the formation of the bar and starburst activity.

★ E-mail: jimenaro@fcaglp.unlp.edu.ar

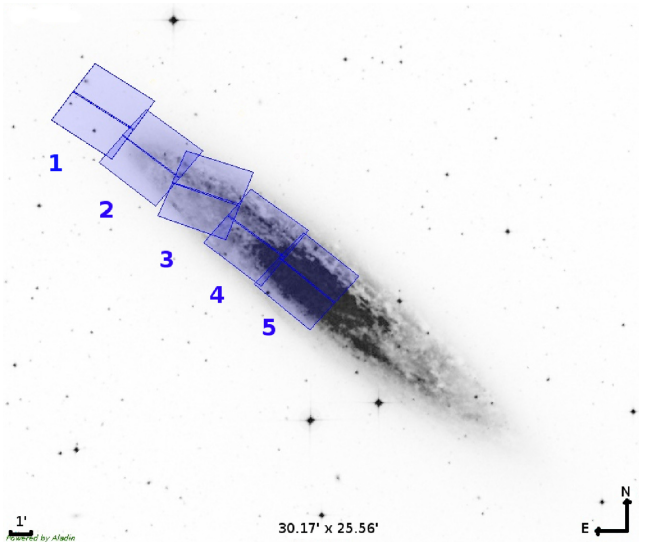

Figure 1. Distribution of the different *HST*/ACS fields (rectangles) used in this work overlaid on a digitized sky survey (DSS) image of NGC 253. North is up and east is left; the image covers 30.1× 25.5 arcmin.

Several young clusters were identified in the nuclear star-forming region of the galaxy (e.g. Watson et al. 1996; Fernández-Ontiveros, Prieto & Acosta-Pulido 2009). One of them was associated with a super star cluster of $\sim 1.4\,x\,10^7$ M$\odot$ and an estimated age of 5.7 Myr. The simultaneous presence of red supergiants and OB stars in this cluster reveals several epochs of star formation (Kornei & McCrady 2009). Davidge (2016) found distinct substructures in it, suggesting that it is a star-forming complex and not a single cluster.

The starburst activity added to its proximity make this galaxy an interesting candidate for the study of its young star population. In spite of this, no young star structures have been detected outside its central region. In this work, we carried out for the first time a search for and identification of young groups in NGC 253 adopting an automatic and objective searching method, and its subsequent analysis. We took advantage of the excellent-quality data from the *Hubble Space Telescope* (*HST*) that cover approximately the north-east side and the centre of the galaxy (see Fig. 1).

The paper is organized as follows: In Section 2 we describe the observations and data sets, together with the reduction and data set-up. In Section 3 we present the methods that we used to search for and identify young stellar structures. Section 4 presents our analysis of the detected groups. We discuss our results in Section 5. Finally, in Section 6 we summarize our work and note our main results.

2 DATA

2.1 Observations

The images used in this work were acquired from the Hubble Legacy Archive[1] and were obtained in 2006 September, as part of the programme GO-10915 (principal investigator: J. Dalcanton), during *HST* Cycle 15. These observations correspond to five fields of NGC 253, and were carried out with the wide-field camera (WFC) of the Advanced Camera for Surveys (ACS). The WFC has a mosaic of two CCD detectors with a field of view of 3.3 × 3.3 arcmin and a scale of 0.049 arsec pixel^{-1}. The five fields cover a total length of approximately 16 arcmin encompassing more than half of the galaxy (see Fig. 1). Three broad-band filters were used (F475W, F606W and F814W), with total exposure times of 1482 s, 1508 s and 1534 s, respectively, except field 1, which has higher exposure times: 2256 s (F475W), 2283 s (F606W) and 2253 s (F814W).

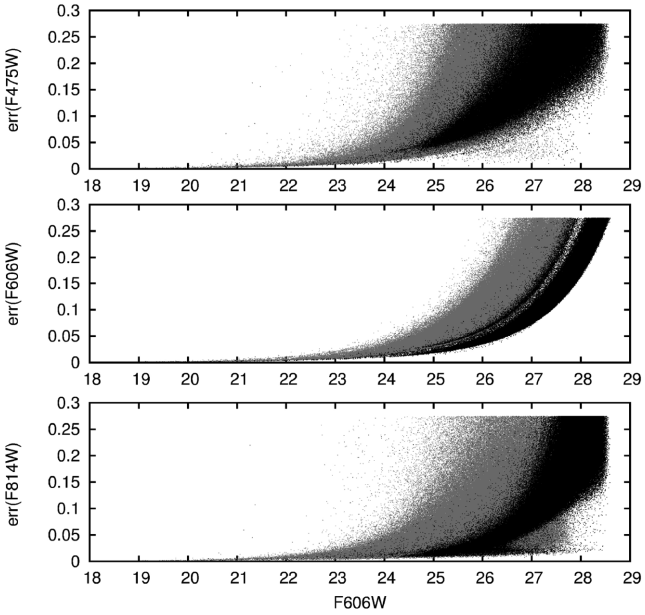

Figure 2. Photometric errors in the bands F475W (top), F606W (middle) and F814W (bottom) versus F606W magnitude for fields 1 (black) and 5 (grey).

2.2 Photometry

Binary FITS (Flexible Image Transport System) tables of photometry were obtained from the database of the Space Telescope Science Institute (STScI).[2] They correspond to the 'star files' from the ACS Nearby Galaxy Survey (ANGST). These files contain the photometry of all objects classified as stars with good signal-to-noise values (S/N > 4) and data flag < 8. These data were obtained performing point-spread function (PSF) photometry using the package DOLPHOT adapted for the ACS camera. The reduction procedure is explained in detail in Dalcanton, Williams & ANGST Collaboration (2008). In Fig. 2 we show the photometric errors in the different bands for fields 1 and 5, which are, respectively, the fields with the lowest and highest stellar densities. To evaluate the completeness of the data, we built the luminosity function (LF) for the five studied fields (see Fig. 3). The number of stars per bin starts to decrease at F606W ∼ 26.5. Therefore we consider that the sample is complete up to this value.

2.3 Photometric correlation of tables

Three photometric tables per field (in total 15 tables) were obtained from ANGST, each one providing photometric information on only two bands. In order to join the three magnitudes in a single table for the fields, we used the code STILTS[3] to perform a cross-correlation (with logical 'OR') between tables with F606W−F475W bands

[1] http://hla.stsci.edu/

[2] MAST: https://archive.stsci.edu/

[3] http://www.star.bris.ac.uk/∼mbt/stilts/

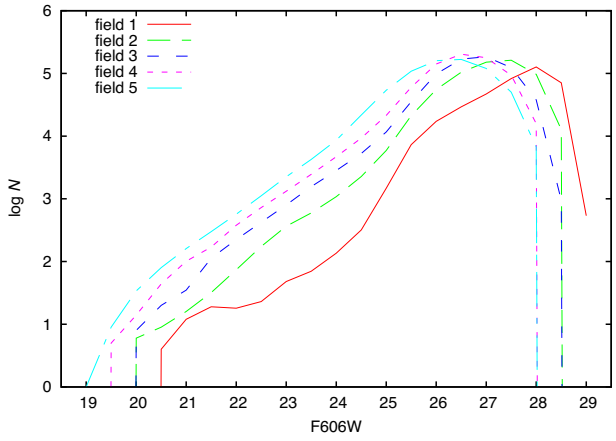

Figure 3. Observed LFs. There is a curve for each studied field.

Table 1. Astrometric (top table) and photometric (bottom table) corrections applied to obtain the final catalogue (see text for details). The first column is (field shifted)–(field to coincide); *N* is the number of stars in the two fields.

Field	$\Delta\alpha\cos(\delta)$ [arcsec]	$\Delta\delta$ [arcsec]
5–Gaia	−0.056	0.078
4–5	0.278	−0.480
3–4	0.252	0.285
2–3	−0.022	0.022
1–2	−1.055	−0.096

Field	ΔF475W	ΔF606W	ΔF814W	*N*
4–5	0.011 ± 0.082	0.036 ± 0.073	0.047 ± 0.081	221
3–4	0.119 ± 0.183	0.081 ± 0.115	0.047 ± 0.099	45
2–3	−0.076 ± 0.119	-0.015 ± 0.082	−0.003 ± 0.067	162
1–2	−0.001 ± 0.015	-0.042 ± 0.017	0.047 ± 0.017	2

and those with F814W−F606W bands, obtaining five photometric tables, one for each field.

Furthermore, the adjacent fields slightly overlap with each other (see Fig. 1); therefore we used STILTS to merge the information on the five fields into one single table with approximately 3 x 10^6 objects. For this purpose, for the objects in the overlap region we took a final magnitude that results from the average between the stars in each field. Then we slightly shifted the coordinates of all the fields to agree with those given in Gaia Data Release 1 (Gaia Collaboration et al. (2016); see Table 1).

3 IDENTIFICATION OF YOUNG GROUPS

As a previous step to identify star groups over the galaxy field, it was necessary to study a couple of problems present in our data sample as follows:

(i) Although the ACS/*HST* provides images with a high spatial resolution (∼0.05 arcsec), it is possible that, in the crowded regions of NGC 253, some objects identified as single sources are really blends of two or more, or even compact star clusters.

(ii) NGC 253 is heavily obscured at visible wavelengths, especially in its central region, due to its large amounts of dust (Pence 1980). This causes the detected objects to appear redder than they really are, making it difficult to identify young blue star populations.

3.1 The blending problem

Several previous works have studied this problem (e.g. Renzini 1998; Kiss & Bedding 2005). In our case, to obtain a measure of the importance of the blending effect, we followed the reasoning presented by Kiss & Bedding (2005). Therefore, we performed several numerical simulations using randomly distributed stars with a uniform spatial distribution, a power-law distribution in brightness, ranging from 18–27 mag., and a uniform distribution in colour, ranging from 0–2 mag.. We analysed different stellar density cases ranging from 1 star arcsec^{-2} to 10 star arcsec^{-2}. This range of values corresponds to those found along the galaxy, but we note that the highest ones were only present in a few special places of the galaxy (see Fig. 8 below). Therefore, for a given stellar density value, we build the corresponding bidimensional spatial histograms with a binning step of 0.07 arcsec to obtain binned areas that simulate the ACS/*HST* resolving power. We could then evaluate the total amount of objects with blending in each simulation. To evaluate the error in magnitudes and colours due to this effect, we computed the total magnitude and colour in each bin and compared these values with those corresponding to the brightest star in that bin. The above procedure was repeated 500 times for each stellar density. As a result, we found that the error in magnitude, as expected, increases with the stellar density value. Therefore, in the worst case (10 star arcsec^{-2}), we found that the percentage of stars that had an error in magnitude greater than 0.1 mag increased from almost null values for bright stars (F606W ∼ 18) to only 2 per cent for stars of magnitude F606W = 24. Regarding the behaviour in colour, we found, again for 10 star arcsec^{-2}, that at most 15 per cent of the stars have errors in colours larger than 0.1 mag and this value was approximately independent of the magnitude value. These obtained figures for both errors in magnitude and colours revealed that, although the blending effect was still present using ACS/*HST* data, the amount of stars that reached errors of 0.1 mag were only a small fraction of all the objects, at least for the stellar densities studied.

3.2 The absorption problem

To estimate the visual absorption (A_V) along the galaxy, we selected the brightest objects (F606W < 24) and compared their locations on the colour–magnitude diagrams (CMDs) with the theoretical evolutionary model PARSEC version 1.2S (Tang et al. 2014) with $Z = 0.0152$ corresponding to 10^7 yr. Assuming as a first approximation that all the selected brightest objects belong to the main sequence, it was possible to deredden their location on the CMDs and estimate approximately their individual absorption values. This procedure could include intrinsically red stars that would produce overestimated A_V values. Therefore, we minimized this effect, and a possible blending effect, assigning to each star the minimum A_V value in a surrounding spatial region with at least 10 stars. We adopted a single isochrone to obtain the absorption values for a sample of stars that could cover a wide range of ages and/or metallicities.

The results of the indicated procedure could be sensitive to the crowding/blending present in the galaxy and/or to the adopted isochrone model. To check the former issue we computed the absorption maps for three F606W magnitude ranges (8.8–23.2; 23.2–23.7 and 23.7–24.0) in such way that we have the same amount of stars (11 222) for each group. The obtained absorption maps did not show significant differences among themselves or with the map obtained considering the entire range of bright stars (F606W < 24). The comparison of the different maps allowed us to estimate an error in our results of $e_{A_V} \sim 0.09$ mag. On the other hand, our numerical

simulations (see Section 3.1) and the use of different isochrones revealed that the procedure employed to estimate the absorption values along the galaxy provides enough precision for a first search of young star groups.

In the left-hand panel of Fig. 4 we present the obtained absorption map of the observed region of NGC 253 following the above procedure. In this figure we have not included the most external field (field 1, see Fig. 1), because it presented several foreground stars or background galaxies and very few bright stars belonging to the galaxy, so it would introduce many spurious detections. The obtained absorption map was then used to correct the observed magnitudes of the brightest objects, $(\mathrm{F475W})_0 = \mathrm{F475W} - A_{\mathrm{F475W}}$; $(\mathrm{F606W})_0 = \mathrm{F606W} - A_{\mathrm{F606W}}$ and $(\mathrm{F814W})_0 = \mathrm{F814W} - A_{\mathrm{F814W}}$. For this task, we use the corresponding absorption value for each filter, which were estimated using the coefficients $A_{\mathrm{F475W}}/A_V = 1.192$, $A_{\mathrm{F606W}}/A_V = 0.923$ and $A_{\mathrm{F814W}}/A_V = 0.605$[4] (O'Donnell 1994). In the right-hand panel of Fig. 4 we show a *WISE*[5] IR false-colour image of the same NGC 253 region shown in the left-hand panel. It was obtained from the combination of the W3 and W4 bands, which best map the dust content. We could note that the regions with stronger absorption correspond to the brightest areas (highest dust content); these are the nucleus, the bar, and the innermost spiral arms.

3.3 Selecting blue and red objects

To split the selected brightest objects between intrinsic blue ones and those probably identified with red stars, we used the following criteria: a) $\mathrm{F475W}_0 - \mathrm{F606W}_0 < 0.5$ and $\mathrm{F606W}_0 - \mathrm{F814W}_0 < 0.5$ for adopted *blue objects*, and b) $\mathrm{F475W} - \mathrm{F606W} > 1$ and $\mathrm{F606W} - \mathrm{F814W} > 1$ for adopted *red objects*. For this last group we considered only those objects that were not include in the blue sample. It is important to note that the first group (a) was selected using the corrected magnitudes, the red objects (b) instead were selected using the observed magnitudes. We then used the *blue objects* to detect young star groups. A combination of Hess diagrams and CMDs of all the detected objects is shown in the top panel of Fig. 5. In the bottom panel we show the CMDs of each selected group where the diffuse border between *blue* and *red objects* reveals the strong dispersion of the absorption values present along the galaxy.

3.4 Searching method

With the aim of identifying young star groups in NGC 253, we employed the path linkage criterion (PLC; Battinelli 1991) over the *blue objects* selected above. The main idea of the technique is that two objects belong to the same star group if it is possible to connect them by successive links of *blue objects*. The link distance between selected objects must not be larger than a fixed parameter called the search radius d_s. A young star group is detected when it is possible to link more than p objects. To adopt adequate values for the parameters d_s and p, we plot in Fig. 6 the number of identified groups using the PLC as a function of d_s for different p values. A good choice for the parameter d_s is set by the maximum number of groups detected for a given p value (Pietrzyński et al. 2001). Fig. 6 reveals that this maximum is located for d_s between 1.5–2 arcsec. Based on these values, and taking care to detect the smallest subgroups of each large association or stellar complex, we adopted a more extended range of d_s, covering the range 0.3–2 arcsec ($\sim$ 5–34pc at 3.56 Mpc; Tully et al. 2013). Using this criteria, the method identified first the smallest groups using $d_s = 0.3$ arcsec, then this value was increased using a step of 0.4 arcsec and the PLC method was run again over the remaining *blue objects*. This procedure was repeated until d_s reached a value of 2 arcsec. Regarding the parameter p, it must be chosen prudently. While a low value results in many spurious detections, a high one may cause the loss of the smallest groups. We then studied the results obtained for different p values (see Fig. 6). We also noticed that, in a similar study for the NGC 300 galaxy, Rodríguez et al. (2016) adopted $p = 10$ stars; however, for NGC 253 we are leading with a more distant galaxy and there is probably a blending effect with the individual objects in the ACS images used. Therefore, we considered $p = 8$ objects as a reasonable value.

Employing the described procedure, we detected 897 individual groups of young objects. However, a few of these groups were spurious detections caused by bright foreground stars, which caused noise spikes in the extended PSFs, or background galaxies, which were identified as faint extended diffuse objects. These false detections were located mostly in fields 1 and 5. Removing these spurious detections manually, we obtained a final list of 875 young star groups. These groups are show in Fig. 7 over an infrared *WISE* false-colour image of the galaxy. The good agreement between their distribution and the large galactic structures of the galactic spiral arms and the central bar can be noted (see Sections 3.6 and 5.3).

3.5 Stochastic detections

To evaluate the fraction of star groups found using the PLC that could be stochastic gatherings of stars and not real groups, we ran numerical simulations using randomly distributed sources with similar star densities to three selected regions, which have very different stellar density values. These are: 1) the region at $\sim$2 arcmin north-east of the galactic nucleus, 2) a place in one of the spiral arms, and 3) a region between the spiral arms. In each region we measured the mean stellar density of the *blue objects*, and we respectively found the following values: 1) $\rho = 0.635$ star arcsec^{-2}, 2) $\rho = 0.203$ star arcsec^{-2} and 3) $\rho = 0.028$ star arcsec^{-2}.

The first region is the densest, close to 0.64 *blue objects* per arcsec. This high density means that the average distance among stars is 0.70 arcsec. So, setting the PLC algorithm to a similar search radius or greater, the method will find all the stars belonging to one single cluster that is a collection of all the stars. Using 03, the lowest search radius that we have used for the real data, we found one stochastic cluster in four cases from 10 000 experiments, a very low number. Increasing the d_s value, the obtained numbers were still low, for example for $d_s = 0.4$ arcsec we found 149 clusters in 10 000 experiments. We noticed that the stellar groups found by the PLC over the numerical simulations had 'worm' shapes. This means that they seemed to be an extended twisted line, and they did not have any circular shape as would be expected for real star groups. Therefore, most of the stochastic clusters did not pass a simple visual inspection. We did not find any stochastic clusters for cases 2) and 3) for $d_s = 0.3$ arsec and very few for a higher search radius.

[4] http://stev.oapd.inaf.it/cgi-bin/cmd
[5] http://wise.ssl.berkeley.edu/

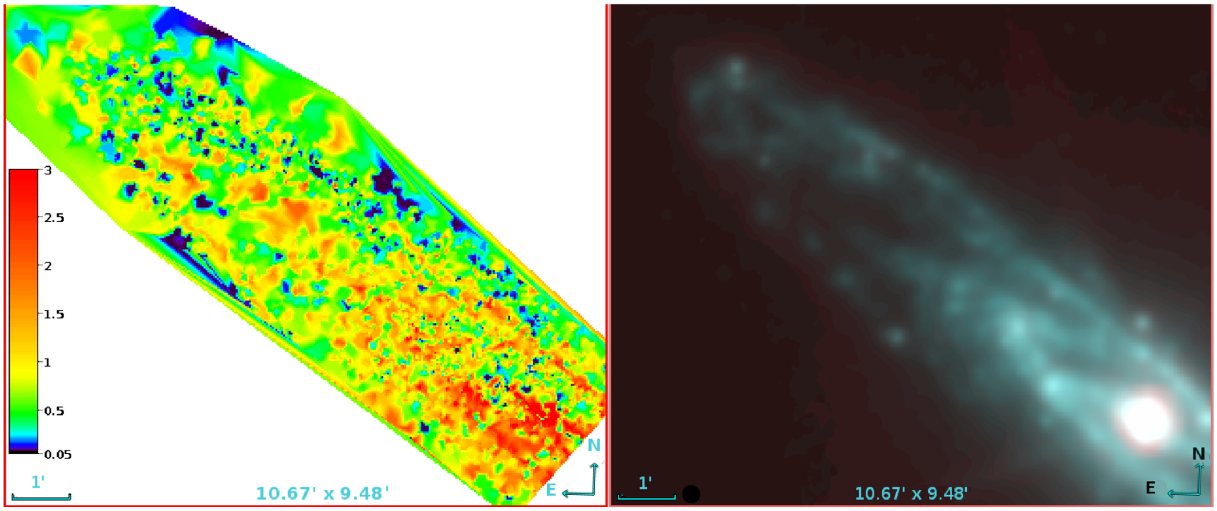

Figure 4. Left: Visual absorption (A_V) map of the observed region of NGC 253. Right: *WISE* IR colour image of NGC 253, obtained by the combination of the W3 and W4 bands. A colour version of this figure and a FITS version of the absorption map are available online.

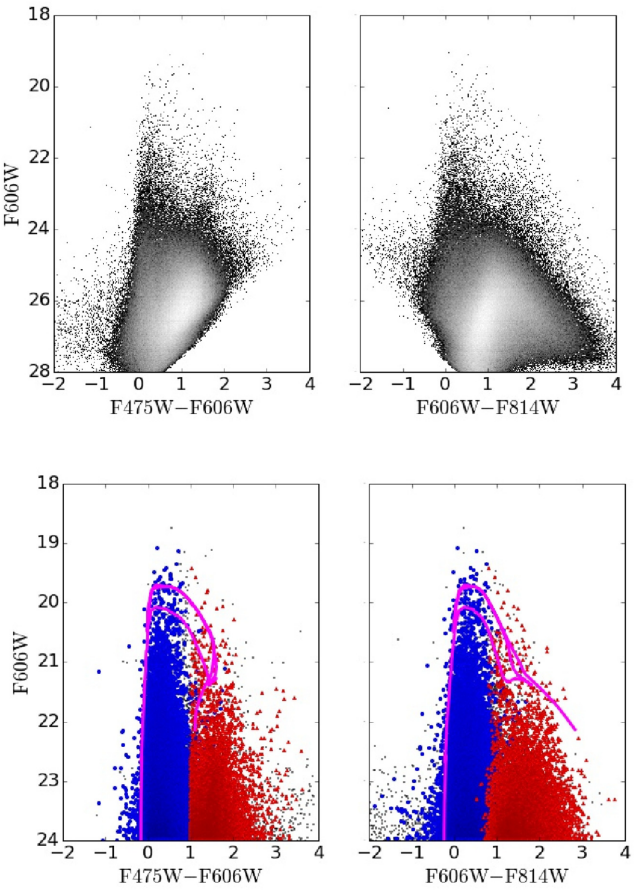

Figure 5. Top panels: Combined Hess diagrams and CMDs with all the detected objects over the total covered region in NGC 253. The different grey shades indicates the stars' relative densities from black (less dense) to white (more dense). Bottom panels: Blue circles and red triangles indicate the selected brightest blue and red objects (see Section3.3). The pink line indicates the PARSEC version 1.2S isochrone Tang et al. (2014) corresponding to 10^7 yr and metallicity $Z = 0.0152$, displaced adopting a distance modulus of $(Vo - M_V) = 27.75$ (Tully et al. 2013), a normal reddening law ($R = A_V/E(B - V) = 3.1$) and a value for $E(B - V) = 0.016$ corresponding to the foreground reddening toward NGC 253 (Schlafly & Finkbeiner 2011). A colour version of this figure is available online.

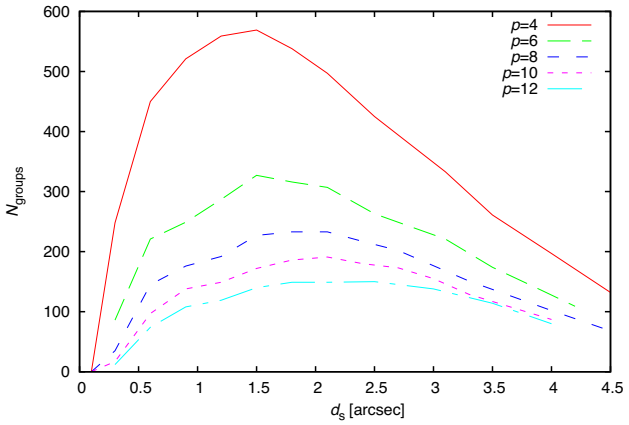

Figure 6. Behaviour of the number of groups detected using the PLC technique as a function of the parameter d_s for different values of the parameter p.

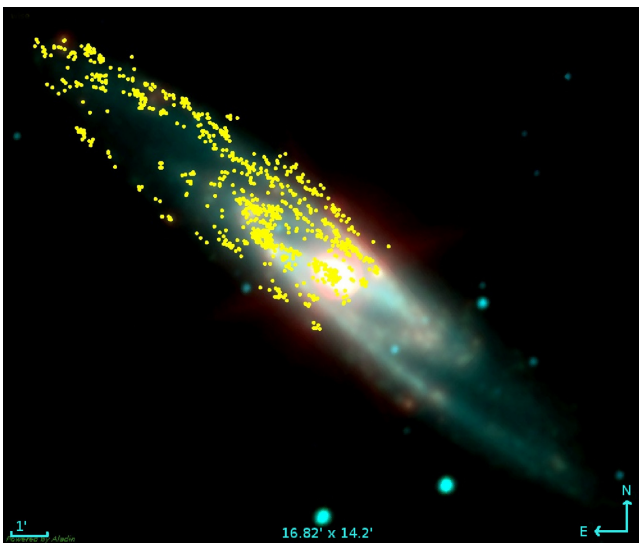

Figure 7. Detected young groups (yellow symbols) over an infrared *WISE* false-colour image of NGC 253. The image covers 16.82 arcmin × 14.2 arcmin, north is up and east is left. A colour version of this figure is available online.

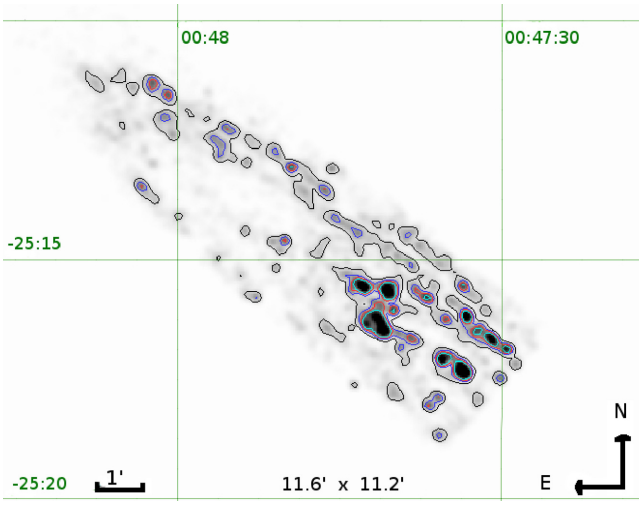

Figure 8. Stellar density map of blue stars; the overlapping contours correspond to different density levels: 40, 80, 110, 145 stars per bin of 8×8 arcsec^2. The image field is 11.6× 11.2 arcmin, north is up and east is left. Colour and FITS versions of this figure are available online.

3.6 Identifying large young structures

Larger young stellar structures could be found using the PLC with an even larger search radius or by building the stellar density map. We choose this last option since it produces better and clearer results.

To build the corresponding density map we constructed a two-dimensional histogram counting the numbers of objects in spatial bin sizes 8×8 arcsec^2. Then, we applied the drizzle method considering a 2.0 arcsec step (see Fruchter & Hook 2002 for details of this method). Over this map we plotted isodensity at several values: 40, 80, 110, and 145 stars per bin of 8×8 arcsec^2.

The stellar density map with the different contours is presented in Fig. 8. Here we can also identify how the blue population delineates the spiral arms of the galaxy. Furthermore, the way in which larger structures enclose smaller and denser ones point to a hierarchical behaviour of the young population. We will discuss this result in Section 5.2.

4 ANALYSIS

We performed an automatic analysis of the detected young star groups using a numerical code developed in FORTRAN 95. This code allowed the study of selected groups in a systematic and homogeneous way. The code estimated the basic parameters of each group detected by the PLC, their sizes, densities, and number of object members, and built their CMDs and LFs, with their corresponding slope values.

Table 2 presents the first ten rows of the resulting catalogue, in which are listed the properties for each of the 875 young groups. The complete version is only available online.

4.1 Sizes and densities

The location and size of each group (α_{J2000}, δ_{J2000} and radius, r) were computed, respectively, as the mean and twice the radial standard deviation (σ) of the location of the corresponding objects identified by the PLC method. An approximate value of the group's stellar density could be estimated counting the total numbers of stars in a volume of $\pi\, r^3$ (see Table 2).

4.2 Field star decontamination

To better study each group, our code decontaminated their corresponding CMDs from field stars by performing statistical cleaning. The cleaning method was based on a comparison between the CMD for a young group region and the CMD for a corresponding field region located near that group and covering the same sky area. Therefore, those objects with similar positions over both CMDs were eliminated in the CMD of the group region (see Gallart et al. 2003 for details).

The above procedure was applied taking into account the colour indexes CI1 = F475W − F606W and CI2 = F606W − F814W simultaneously. For each star in the region we calculated the distance in the CMDs with all the stars in the field. The most similar star in the field provided the minimum distance value; if this value was less than a given tolerance, then the star in the group region was subtracted. The CMD distance was calculated using the following expression: $\{(\mathrm{F606W_r} - \mathrm{F606W_f})A\}^2 + \{(\mathrm{CI1_r} - \mathrm{CI1_f})B\}^2 + \{(\mathrm{CI2_r} - \mathrm{CI2_f})B\}^2$, where the subscripts 'r' and 'f' refer to stars in the region and field respectively and the constants A and B are normalization factors.

Table 2. Catalogue of young star groups in NGC 253. Here we present the first ten rows; the complete table is only available in electronic form.

Name	RAJ2000 (deg)	DECJ2000 (deg)	r [pc]	N	N_{dct}[a]	$N_{\mathrm{dct-bri}}$[b]	F606W$_{\mathrm{bb}}$[c]	dens [$*$ pc^{-3}]	LF slope (Γ)	err$_\Gamma$	d_{GC}[d] [kpc]	A_v[e]
AS002	11.911 189	−25.250 842	14.80	48	32	18	19.99	0.003 14	0.12	0.03	3.91	0.610
AS003	11.894 225	−25.283 620	13.77	31	23	19	19.85	0.002 80	0.04	0.05	0.47	0.610
AS004	11.872 012	−25.281 292	15.15	31	20	17	18.45	0.001 83	0.03	0.04	3.07	0.610
AS006	11.881 036	−25.286 077	18.59	54	34	12	20.77	0.001 69	0.02	0.05	1.26	0.050
AS007	11.909 739	−25.280 824	11.36	26	15	9	20.94	0.003 26	0.02	0.05	1.85	0.050
AS008	11.920 171	−25.274 954	8.26	22	16	9	23.12	0.009 03	0.03	0.02	2.58	0.050
AS009	11.888 770	−25.289 815	17.90	46	29	22	20.26	0.001 61	0.02	0.05	0.24	0.050
AS010	11.958 507	−25.243 423	23.41	105	71	44	19.18	0.001 76	0.21	0.03	5.05	0.190
AS011	11.877 059	−25.280 397	10.33	24	18	11	21.80	0.005 20	0.07	0.04	2.58	0.190
AS012	11.910 848	−25.277 194	12.74	35	27	18	19.77	0.004 16	0.10	0.05	1.72	0.190

Notes:
[a]The subscript 'dct' indicates stars belonging to the decontaminated region. [b]The subscript 'bri' indicates bright stars with F606W < 24.
[c]F606W$_{\mathrm{bb}}$ is the F606W value of the brightest blue object in the group.
[d]d_{GC} is the galactocentric distance.
[e]A_v is the characteristic absorption affecting the group.

In order to obtain a field region as homogeneous as possible, avoiding possible neighbour groups or falling outside the field of view, the code choose five different field regions for each group. The first region is a ring around the studied group, and the others are selected as follows: $(\alpha_0 \pm \Delta\alpha, \delta_0)$; $(\alpha_0, \delta_0 \pm \Delta\delta)$, where $\Delta\alpha = \Delta\delta = 11.6$ arcsec $\sim$ 200 pc. Then the fields with the maximum and minimum number of stars were discarded, and the final decontamination result is an average of the decontamination obtained with the three remaining field regions.

4.3 Colour–magnitude diagrams

We built the decontaminated CMDs, F606W versus F475W − F606W and F606W versus F606W − F814W for each star group, taking into account the blue and red populations identified in Section 3.3.

In Fig. 9 we show the CMDs of three young groups. We overlapped the evolutionary models of PARSEC version 1.2S corresponding to 10^7 yr (grey line) and 10^9 yr (pink line) with solar metallicity for comparison. These models were displaced adopting a distance modulus of $(Vo - M_V) = 27.75$ (Tully et al. 2013), a normal reddening law ($R = A_V/E(B-V) = 3.1$) and a value for $E(B-V) = 0.016$ corresponding to foreground reddening toward NGC 253 (Schlafly & Finkbeiner 2011). In these diagrams we can note that a small group of *red objects* still prevails. This is because in the right-hand regions of the diagrams the stars are more dispersed, causing the statistical subtraction to lose efficiency. Nevertheless, we can see that for the *blue objects* the statistical subtraction is more reliable.

4.4 Luminosity function

The F606W LF of the brightest end of each detected young group was built using only the selected *blue objects* inside the corresponding radius r (see Section 3.3) and adopting a bin interval of 0.5 mag. The LF slopes, $\Gamma = \mathrm{d}\log N/\mathrm{d}\,\mathrm{F606W}$, were determined performing a linear least-squares fit. The obtained slopes are listed in Table 2.

In Fig. 10 we present the LFs for the groups AS150, AS352 and AS855; the straight lines indicate the linear fits and the indicated errors correspond to $N^{1/2}$, where N is the number of stars in each 0.5 mag bin.

The mean slope was derived considering only the groups with more than 30 bright members and $\mathrm{err}_\Gamma \leq 0.05$, obtaining a value of 0.21.

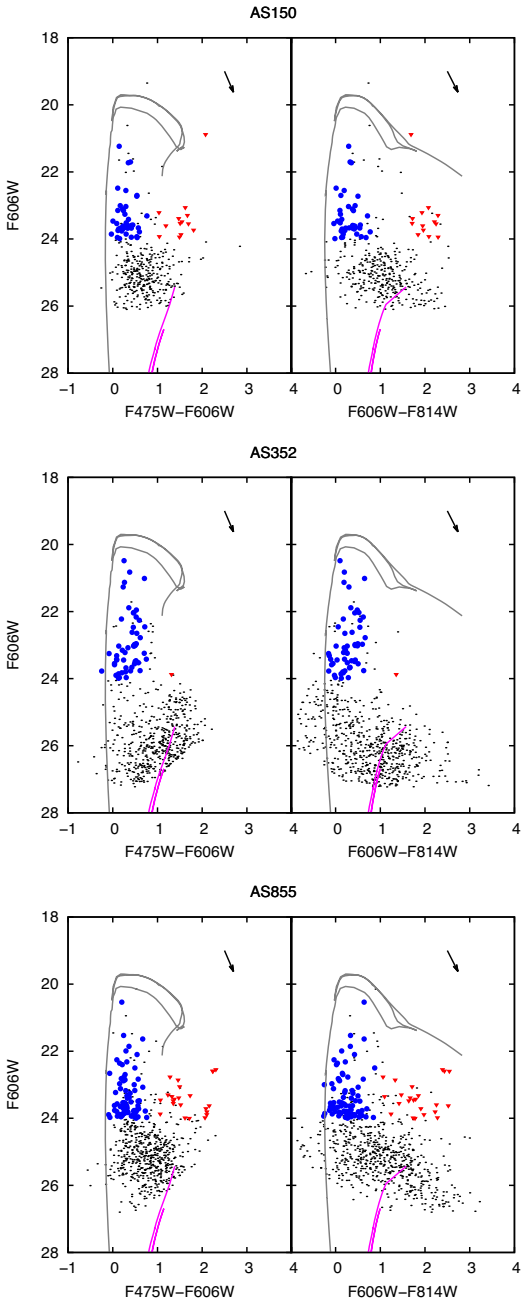

Figure 9. Decontaminated CMDs F606W versus F475W − F606W and F606W versus F606W − F814W of the star groups AS150, AS352, and AS855, which are located at different galactocentric distances. The meaning of symbols is explained in the text (Section 4.3). The grey and pink lines indicate the isochrones corresponding to 10^7 yr and 10^9 yr respectively and metallicity ($Z = 0.0152$). (Tang et al. 2014). The arrow indicates the reddening vector. A colour version of this figure is available online.

5 DISCUSSION

5.1 Comparison with NGC 300

We compared the young groups that we detected with those identified in NGC 300, which were studied by Rodríguez et al. (2016) using similar observational data to those in the present work.

In Fig. 11 we plot the number of star members versus the size of the groups in each galaxy. To be consistent with Rodríguez et al. (2016) we adopt in this figure a radius of 1σ (the radial standard deviation of the group member location). We performed a quadratic fit to the data, in order to compare the numbers of members detected in groups of the same size in both galaxies. A least-squares fit was performed, taking into account groups with sizes larger than 9 pc, to avoid the most crowded regions. We found a ratio of ~ 2 between the quadratic coefficients (α) of each galaxy. In other words, the associations in NGC 300 would appear to contain twice as many stars as NGC 253.

However, NGC 300 is located almost half the distance to NGC 253; therefore in this galaxy we were reaching less luminous objects than in NGC 253, or less-massive main-sequence stars. Thus, it was expected that we would detect more members in the NGC 300 associations, but this was only a distance effect.

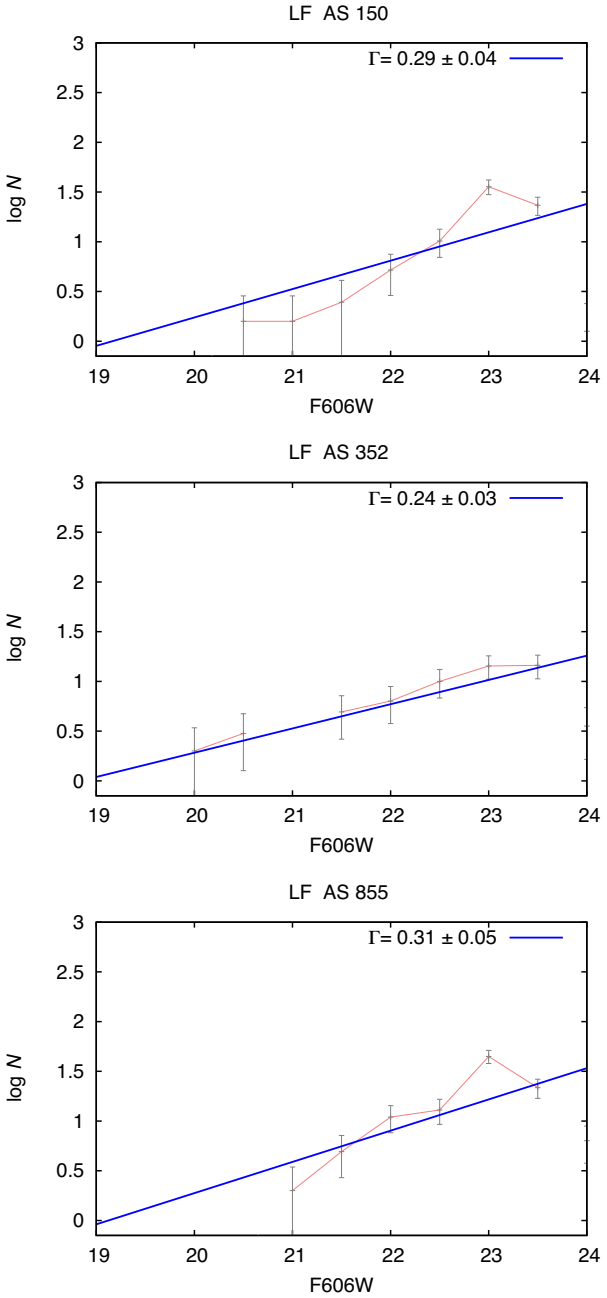

Figure 10. LF of three young star groups located at different places in the galaxy, AS150, AS352 and AS855. The line indicates a linear fit over the considered bins (see Section 4.4); the slope estimated in each case is indicated in the top-right-hand corner.

5.2 Hierarchical structure in NGC 253

As was mentioned in Section 1, star-forming regions exist in a wide range of sizes, from compact star clusters to the spiral arms of a galaxy. Using the PLC and the stellar density map (Sections 3.4 and 3.6), we have searched for and identified an important number of young star groups whose sizes and amount of members reveal that they include different kinds of structures, from simple open clusters to important complexes of several OB associations. In Fig. 8 we can see how the largest and most scattered young structures enclose the densest and compact ones, going through different density levels, indicated by the different contours. In fact, if we plot the PLC groups

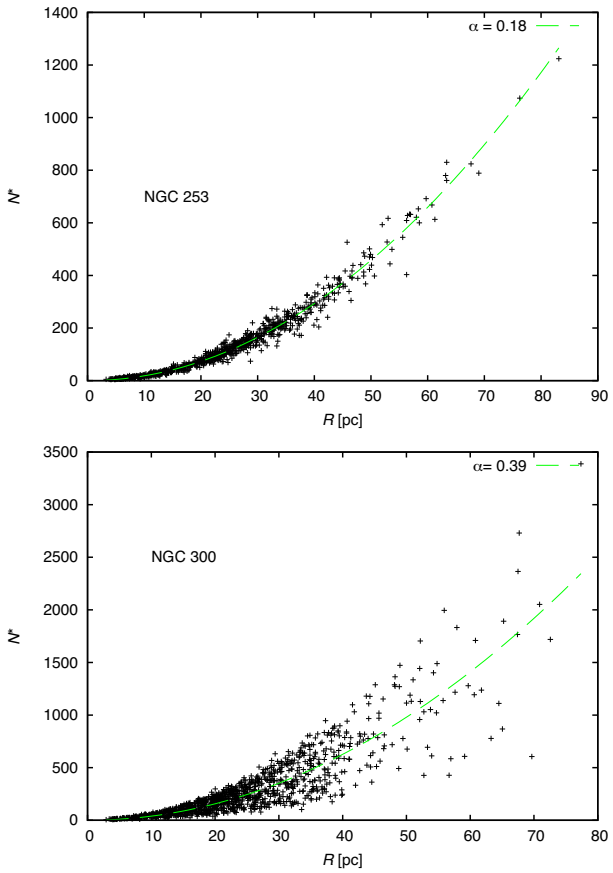

Figure 11. Number of star members versus radius of young groups, for NGC 253 (top) and NGC 300 (bottom). The dashed lines correspond to a quadratic fit over the data.

together with the contours obtained from the density map, we see a large number of these groups within the densest contours (see Fig. 12), suggesting that they enclose stellar complexes.

This behaviour of the young population is known as hierarchical structure (e.g. Elmegreen et al. 2000). We can see the relationships among these structures in Fig. 13, in which we present the corresponding tree diagram or dendrogram. At the bottom, the diagram starts with the structures detected in the lower density level (40 stars per bin of 8 × 8 arcsec^2, black contour in Fig. 8). Most of these structures divide themselves into denser and smaller systems that are detected in the second density level (80 stars per bin of 8 × 8 arcsec^2, blue contour in Fig. 8). This behaviour is repeated through the denser levels (110 and 145 stars per bin of 8 × 8 arcsec^2, red and turquoise contours respectively). Finally, we add a fifth level, which corresponds to the groups detected with the PLC method and which are contained in the structures detected in level 4. It is not possible to detect such groups in the density map because the map pixel sizes is 2 arcsec, which is comparable to the group size.

5.3 Distribution of the young star groups in the galaxy

As was indicated in Section 3.4, in Fig. 7 we show the distribution of the identified groups on an infrared *WISE* image of the galaxy. Therefore, it is possible to note that the stellar groups are mainly located over some special features of NGC 253, I) the nuclear region, II) the observed extreme of the bar, III) a ring-like structure enclosing the bar, and IV) the spiral arms. All these structures are

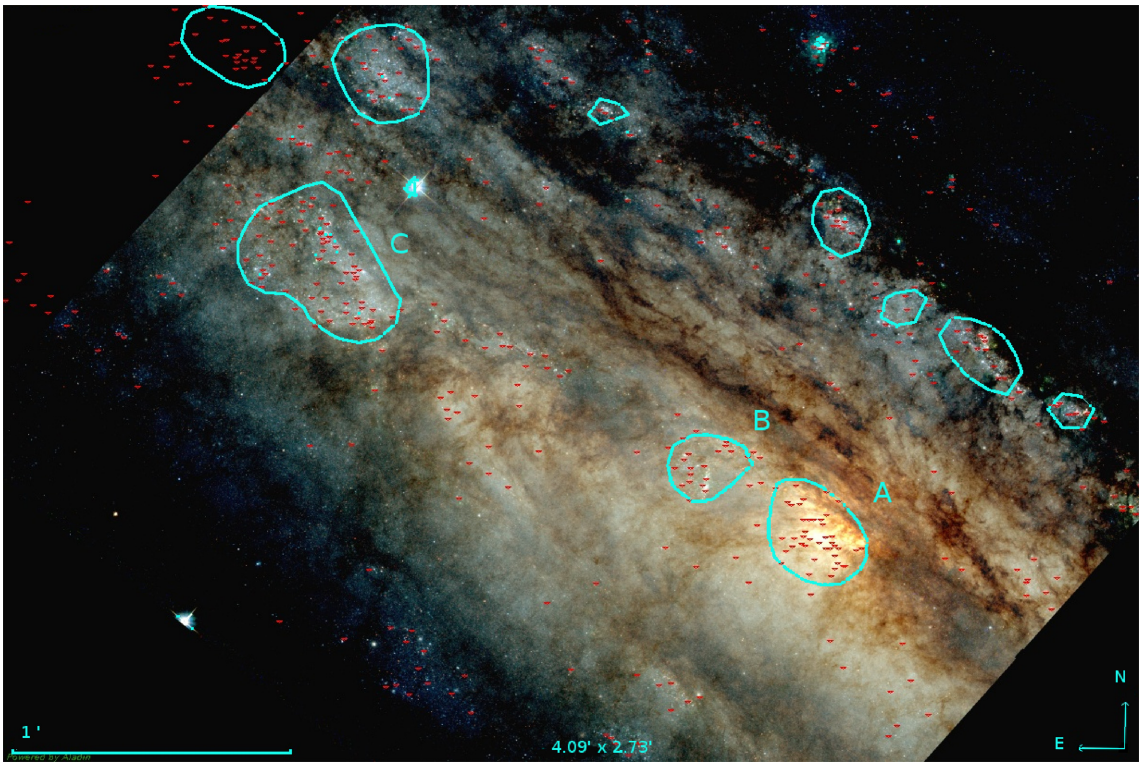

Figure 12. ACS/WFC colour image of field 5, obtained from the combination of the filter F475W in blue, F606W in green and F814W in red using Aladin. The inverted triangles indicate the centre of the individual groups detected by the PLC method; the contours are the densest that appear in Fig. 8 and indicate stellar complexes (see Sections 5.2 and 5.3). A colour version of this figure is available online.

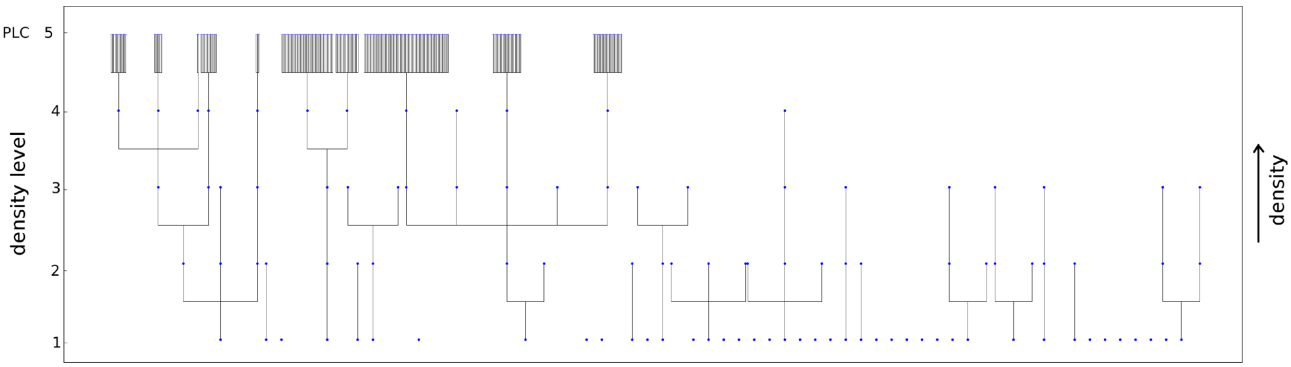

Figure 13. Dendrogram of the young stellar structures detected at different density levels. Levels 1–4 correspond to 40, 80, 110, and 145 stars per bin of 8 × 8 arcsec^2, respectively. Level 5 corresponds to the most compact groups detected using PLC. The small circles indicate different stellar structures. Structures that are related in a hierarchical way are connected by solid lines.

prominent in the near-infrared spectral range (see fig. 4 of Iodice et al. 2014).

In particular, we found two stellar complexes with almost 20 members (individual young groups) near the central region of the galaxy (contours A and B in Fig. 12). The one closer to the centre (complex A) is within the 300 pc of starburst activity, and it is coincident with the super star cluster described in several works (eg. Kornei & McCrady 2009; Davidge 2016). Through the PLC method we could identify several individual star groups in this region, suggesting that it is in fact a stellar complex rather than a super cluster. The same conclusion was arrived at by Davidge (2016), who found star formation in different locations inside this region.

We can also see in Fig. 7 a large stellar complex containing several groups at the edge of the bar; this complex is indicated with contour C in Fig. 12. In this last optical image the bar is totally obscured by the dust and only the star-forming region at the edge of the bar is visible. This knot and the other extreme of the bar were identified by Iodice et al. (2014) as bright points, in near-infrared images of VISTA,[6] that connect the bar with the outer spiral arms. Their analysis suggests these knots to be regions of local star formation instead of being the typical ansae observed in other barred galaxies, which is consistent with our detections.

[6]http://www.vista.ac.uk/

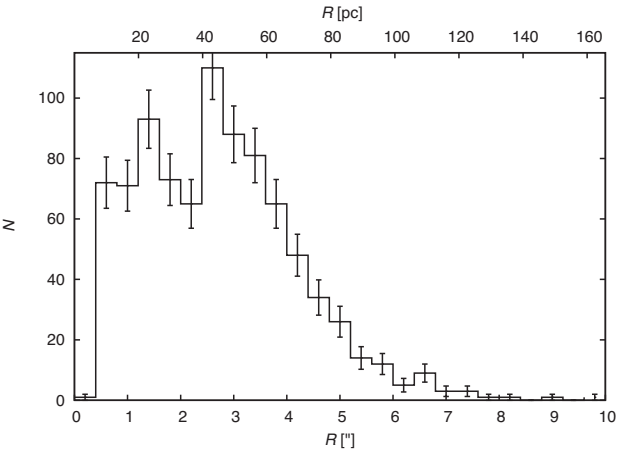

Figure 14. Size distribution of young star groups in NGC 253. Sizes in parsecs (upper edge) were computed using a distance of 3.56 Mpc (Tully et al. 2013).

On the other hand, we expected to find young groups in the ring structure, since this region is associated with active star formation as was suggested by the H α maps of the region (Hoopes, Walterbos & Greenwalt 1996). The origin of this structure, with a radius between 2.6 and 3.1 kpc, is not yet well understood. According to Iodice et al. (2014) it is probably the result of a merge with a small satellite or, alternatively, it is an intermediate phase in the bar formation.

5.4 General properties of the young star groups

In Fig. 14 we show the size distribution of the star groups; we can see that the radius ranges from 5–150 pc with a peak close to 40 pc. We found an average radius of $\sim$ 47 pc. These values are in good agreement with the OB association size found in other galaxies, using automatic search methods and *HST* images. Rodríguez et al. (2016) found a value of 25 pc for the mode and the average radius of young star groups in NGC 300; although these values are lower than ours, we must consider that they used values of radius equal to 1σ instead of 2σ as in this work. Bresolin et al. (1998) studied the OB associations in seven spiral galaxies, NGC 925, NGC 2090, NGC 2541, NGC 3351, NGC 3621, NGC 4548, and M101, finding size distribution peaks between 25 and 45 pc and an average radius between 25 and 60 pc. In our Galaxy these values are somewhat smaller. Mel'Nik & Efremov (1995) found a maximum in the size distribution of 15 pc and an average radius of 20 pc in the OB associations with distances within 3 kpc of the Sun. For example, the associations in the Orion region Ori OB1a and Ori OB1b have radii of 37 pc and 17 pc respectively (Briceno 2008); the associations in the Cygnus region have an extended range of radii from 10–70pc (Garmany & Stencel 1992).

In Fig. 15 we present the trend of several parameters against the galactocentric distance. In the upper panel we show the F606W magnitude value of the brightest star in the stellar groups for each 0.5 kpc bin; the middle panel presents the behaviour of the red (F814W) background level measured on the ACS/WFC drizzle images; and the bottom panel indicates the stellar density values of bright stars. Both the background levels and the stellar density values correspond to the same stellar groups indicated in the upper panel.

These figures allow us to notice that the brightest stars in the stellar groups decrease up to distances $\sim$6 kpc and then remain

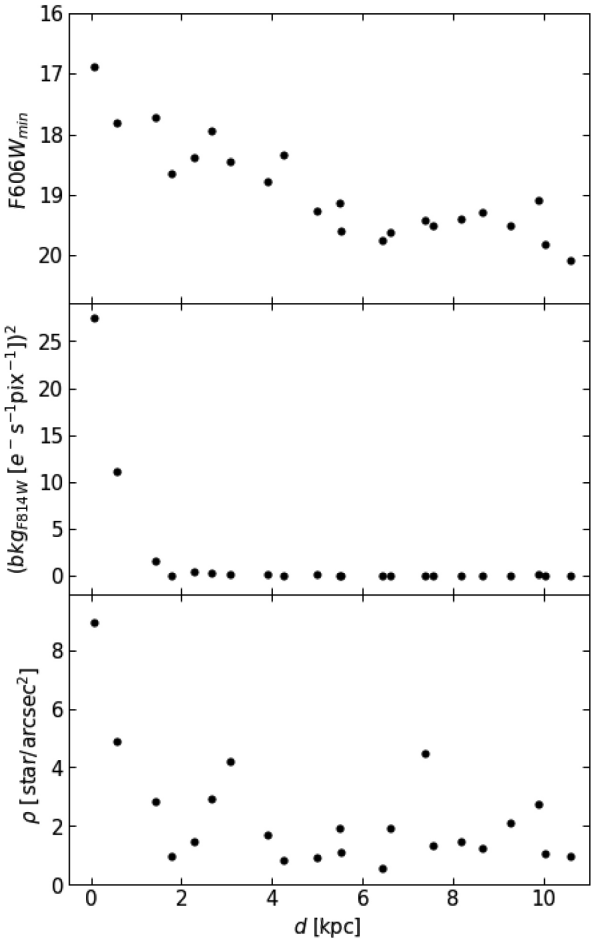

Figure 15. Top panel: Magnitude of the brightest star in the stellar groups. Middle panel: The red (F814W) background level. Bottom panel: The stellar density of stars brighter than F606W = 24, with respect to galactocentric distance. A bin size of 0.5 kpc was used and the same stellar groups were considered in the three panels.

approximately constant. The behaviour in the central part of the galaxy could be due to a blending/crowding effect, a change in the stellar density since it directly affects the chance to obtain a bright star for a given initial mass distribution, or a flatter slope of the mass distribution itself. The middle panel of Fig. 15 was adopted as an indicator of the blending behaviour (Renzini 1998) and reveals that this problem is not important in most regions of the galaxy, as was indicated in Section 3.1, but it could be important for galactocentric distances lower than 2 kpc. On the other hand, the bottom panel of Fig. 15 reveals the changing behaviour of the stellar density. These results suggest that the trend observed in the upper panel could be mainly due to changes in the stellar density. However, in the central part of the galaxy, the blending effect and the high stellar densities could be a problem.

Regarding the stellar mass and bright distribution of the stellar groups, Bresolin et al. (1998) estimated an average V LF slope of 0.61 for the spiral galaxies mentioned at the beginning of this section. This value is considerably higher that our computation of 0.21. This discrepancy may be partly due to the different magnitude cut-off adopted in the slope measure ($M_V \leqslant -4.76$ in Bresolin et al. 1998, and $M_{\rm F606W} \leqslant -3.81$ in our work). Additionally, the Bresolin et al. (1998) galaxies are much more distant than NGC 253 (between 6.7 and 14.5 Mpc), so it is probable that a blending effect is present,

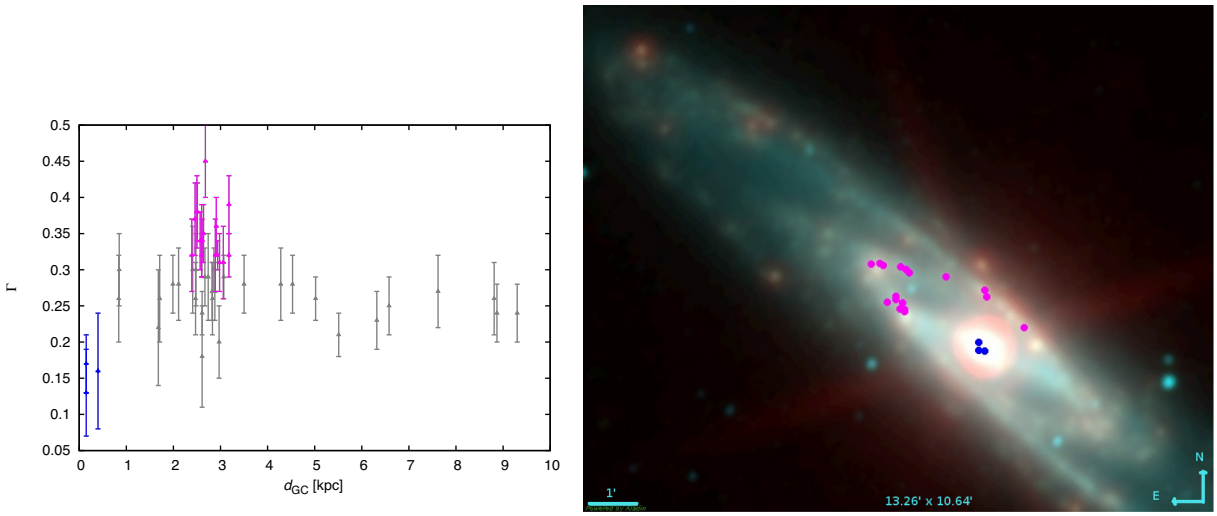

Figure 16. Left: Behaviour of the LF slope with galactocentric distance. Pink dots indicate groups with Γ values greater than 0.3. Blue points are groups with Γ values lower than 0.18. Right: Location of pink and blue dots over a *WISE* IR image of NGC 253. It can be clearly seen that the associations with low-Γ values are found in the galactic core, while those with high values are located over an annular structure surrounding the galactic core.

affecting the object magnitudes and consequently the LF shape. Studying only the most numerous groups with low errors in the fitted slope, i.e. those with more than 50 bright blue stars resulting from statistical decontamination and errors in the slopes lower than 0.09, we found that the groups with low slope values were located near the galactic centre. On the other hand, groups with the highest slope values were located between ∼2 and 3.5 kpc. The left-hand panel of Fig. 16 shows the relationship of Γ and the galactocentric distance; the groups with slope values lower than 0.18 are shown in blue and those with slopes greater than 0.3 are shown in pink. In the right-hand panel of Fig. 16 we overlapped these associations on an IR *WISE* image of the galaxy. In this figure we can note that the groups with low values of the slope are near the galactic centre, within the starburst region and inside complex A (see Fig. 12). These low values indicate that the LF slope is flatter than in the groups of other regions, so there would be more bright stars than in other groups; however, this region is well correlated with the behaviour presented in the middle panel of Fig. 15 and therefore these values could be partially affected by the presence of blending. On the other hand, all the groups with slopes greater than 0.3 are over the annular structure that surrounds the bar and the nucleus; the LFs of these associations are characterized as having a large number of stars of weaker magnitudes.

Additionally, we have estimated a mean density of 0.0006 star pc^{-3} taking into account groups with more than 30 bright stars. It should be noted that this value was estimated counting stars with $M_{F606W} \leqslant -0.8$, which approximately correspond to the spectral type B6.

6 CONCLUSIONS

Using ACS/*HST* images we searched for and identified young star groups in the starburst galaxy NGC 253. For this task, we first derived the absorption affecting different regions of the galaxy. After correcting for this effect, we used the PLC method over the bright blue objects to identify young groups and build a density map to detect larger young structures. A specially designed code was run over the detected groups to estimate their fundamental parameters and to build their corresponding CMDs and LFs.

We constructed a catalogue containing the characteristics of the 875 detected young groups. This catalogue presents coordinates, sizes, number of members, densities, LF slopes and galactocentric distances.

Our study revealed that the groups detected are located over prominent structures of the galaxy, its nuclear region, the edge of the bar, a ring-like structure that encloses the bar, and the spiral arms, confirming that all of them are star-forming regions. The nuclear region of this galaxy had been closely studied due to its starburst activity; it has been associated with a super star cluster by several authors. Nevertheless, we identified almost 20 different groups in this region, suggesting that it is in fact a stellar complex. Additionally we found that this young population has a hierarchical behaviour, in which the smaller groups are contained in larger structures.

The group size distribution revealed a peak near 40 pc and an average radius of 47 pc; these values are consistent with those found in other galaxies. We also estimate a mean value of the F606W LF slope of 0.21, with lower slope values in the galactic centre and higher values in the ring structure, and an average density of 0.0006 star pc^{-3} for stars considered earlier than B6.

ACKNOWLEDGEMENTS

We thank the referee for helpful comments and constructive suggestions that helped to improve this paper. MJR and GB acknowledge support from CONICET (PIP 112-201101-00301). MJR is a fellow of CONICET. This work was based on observations made with the NASA/ESA *Hubble Space Telescope*, and obtained from the Hubble Legacy Archive, which is a collaboration between the Space Telescope Science Institute (STScI/NASA), the Space Telescope European Coordinating Facility (ST-ECF/ESA) and the Canadian Astronomy Data Centre (CADC/NRC/CSA). Some of the data presented in this paper were obtained from the Mikulski Archive for Space Telescopes (MAST). STScI is operated by the Association of Universities for Research in Astronomy, Inc., under NASA contract NAS5-26555. Support for MAST for non-*HST* data is provided by the NASA Office of Space Science via grant NNX09AF08G and by other grants and contracts. This publication makes use of data prod-

ucts from the *Wide-field Infrared Survey Explorer*, which is a joint project of the University of California, Los Angeles, and the Jet Propulsion Laboratory/California Institute of Technology, funded by the National Aeronautics and Space Administration. This research has made use of the Aladin sky atlas developed at CDS, Strasbourg Observatory, France.

REFERENCES

Battinelli P., 1991, A&A, 244, 69
Bedin L. R., Piotto G., Baume G., Momany Y., Carraro G., Anderson J., Messineo M., Ortolani S., 2005, A&A, 444, 831
Bianchi L., Efremova B., Hodge P., Kang Y., 2012, AJ, 144, 142
Bresolin F., Kennicutt R. C. Jr. Stetson P. B., 1996, AJ, 112, 1009
Bresolin F. et al., 1998, AJ, 116, 119
Briceno C., 2008, Reipurth B., ed., Handbook of Star Forming Regions, Volume I: The Northern Sky, Vol. 4, ASP Monograph Publications, p. 838
Chandar R., Bianchi L., Ford H. C., 1999, ApJS, 122, 431
Dalcanton J., Williams B., ANGST Collaboration, 2008, Galaxies in the Local Volume, Astrophysics and Space Science Proceedings, ISBN 978-1-4020-6932-1, Springer, Dordrecht Publication, Springer Netherlands, p. 115
Davidge T. J., 2010, ApJ, 725, 1342
Davidge T. J., 2016, ApJ, 818, 142
Elmegreen B. G., Efremov Y., Pudritz R. E., Zinnecker H., 2000, in Mannings V., Boss A. P., Russell S. S., eds, Protostars and Planets IV, University of Arizona Press, Tucson, p. 179
Engelbracht C. W., Rieke M. J., Rieke G. H., Kelly D. M., Achtermann J. M., 1998, ApJ, 505, 639
Fernández-Ontiveros J. A., Prieto M. A., Acosta-Pulido J. A., 2009, MNRAS, 392, L16
Fruchter A. S., Hook R. N., 2002, PASP, 114, 144
Gaia Collaboration et al., 2016, A&A, 595, A2
Gallart C. et al., 2003, AJ, 125, 742
Garmany C. D., Stencel R. E., 1992, A&AS, 94, 211
Gouliermis D., Kontizas M., Kontizas E., Korakitis R., 2003, A&A, 405, 111
Hoopes C. G., Walterbos R. A. M., Greenwalt B. E., 1996, AJ, 112, 1429
Iodice E., Arnaboldi M., Rejkuba M., Neeser M. J., Greggio L., Gonzalez O. A., Irwin M., Emerson J. P., 2014, A&A, 567, A86
Kiss L. L., Bedding T. R., 2005, MNRAS, 358, 883
Kornei K. A., McCrady N., 2009, ApJ, 697, 1180
Massi F., Giannetti A., Di Carlo E., Brand J., Beltrán M. T., Marconi G., 2015, A&A, 573, A95
Mel'Nik A. M., Efremov Y. N., 1995, Astron. Lett., 21, 10
Moraux E., 2016, EAS, 80, 73
Nantais J. B., Huchra J. P., McLeod B., Strader J., Brodie J. P., 2010, AJ, 139, 1413
O'Donnell J. E., 1994, ApJ, 437, 262
Ott J., Weiss A., Henkel C., Walter F., 2005, ApJ, 629, 767
Pence W. D., 1980, ApJ, 239, 54
Pietrzyński G., Gieren W., Fouqué P., Pont F., 2001, A&A, 371, 497
Pietrzyński G., Ulaczyk K., Gieren W., Bresolin F., Kudritzki R. P., 2005, A&A, 440, 783
Radovich M., Kahanpää J., Lemke D., 2001, A&A, 377, 73
Renzini A., 1998, AJ, 115, 2459
Rodríguez M. J., Baume G., Feinstein C., 2016, A&A, 594, A34
Schlafly E. F., Finkbeiner D. P., 2011, ApJ, 737, 103
Tang J., Bressan A., Rosenfield P., Slemer A., Marigo P., Girardi L., Bianchi L., 2014, MNRAS, 445, 4287
Tully R. B. et al., 2013, AJ, 146, 86
Vučetić M. M., Arbutina B., Urošević D., 2015, MNRAS, 446, 943
Watson A. M. et al., 1996, AJ, 112, 534

SUPPORTING INFORMATION

Supplementary data are available at *MNRAS* online.

av map.fits
catalog.txt
density map.fits

Please note: Oxford University Press is not responsible for the content or functionality of any supporting materials supplied by the authors. Any queries (other than missing material) should be directed to the corresponding author for the article.

This paper has been typeset from a TEX/LATEX file prepared by the author.